IOPscience iopscience.iop.org

Home Search Collections Journals About Contact us My IOPscience

Plume patterns in radiative–convective flows

This article has been downloaded from IOPscience. Please scroll down to see the full text article.

2003 New J. Phys. 5 106

(http://iopscience.iop.org/1367-2630/5/1/106)

View the table of contents for this issue, or go to the journal homepage for more

Download details:
IP Address: 89.201.228.79
The article was downloaded on 29/05/2010 at 05:29

Please note that terms and conditions apply.

New Journal of Physics
An Institute of Physics and Deutsche Physikalische Gesellschaft Journal

Plume patterns in radiative–convective flows

A Parodi[1], **K A Emanuel**[2] **and A Provenzale**[1,3,4]
[1] CIMA, University of Genoa, Via Cadorna 7, Savona, Italy
[2] EAPS-MIT, Cambridge, MA 02139, USA
[3] ISAC-CNR, Corso Fiume 4, 10133 Torino, Italy
E-mail: antonello@cima.unige.it

New Journal of Physics **5** (2003) 106.1–106.17 (http://www.njp.org/)
Received 30 April 2003, in final form 11 July 2003
Published 5 August 2003

Abstract. We study the dynamics of a simplified model of atmospheric convection. The model represents a layer of dry air kept in statistically stationary radiative–convective equilibrium. We discuss the behaviour and the spatial organization of the pattern of convective plumes that emerge in the system, and analyse the intermittency properties of the heat flux field.

Contents

1. Introduction

Mesoscale eddies in the ocean, hurricanes in the tropical atmosphere, cool downdrafts in the ocean thermohaline convection, and strong precipitating updrafts in atmospheric convection are all examples of the intense, localized coherent structures that characterize the dynamics of turbulent geophysical flows.

[4] Author to whom any correspondence should be addressed.

1367-2630/03/000106+17$30.00
© IOP Publishing Ltd and Deutsche Physikalische Gesellschaft

The presence of coherent structures leads to a strong spatio-temporal intermittency of geophysical turbulence, and to an irregular alternation between the localized, high-energy spots of intense dynamical activity—the coherent structures—and the diffuse, more quiescent background. This is certainly the case for vortex-dominated systems in the ocean (e.g., [22, 23] and references therein) and for turbulent convection at large Rayleigh number (e.g., [31, 35]). A spectacular example of intermittent turbulent convection in the atmosphere are the tall cumulonimbi found at the tropics. These cloud towers occupy only a small fraction of space, and are associated with strong updrafts. The downdrafts are much weaker, and occupy the clean air between the cloudy and precipitating updrafts (see, e.g., [12, 18]).

In this paper, we focus on the behaviour of convective updrafts and on the intermittent dynamics of atmospheric convection. Atmospheric convection is, of course, very complicated. If we try to rationalize the behaviour of convective precipitation in terms of model equations, we have to turn attention to the dynamics of moist, precipitating, radiatively cooled convection (see, e.g., [12]). When the problem is approached in its full flavour, one has to cope with cloud microphysics, droplet dynamics, turbulence parametrization schemes, moist thermodynamics and phase changes, and the complexity of the models may grow beyond reach.

Another avenue is based on keeping the description as simple as possible, at the cost of building only a deformed image of the phenomenon under study. From this point of view, one could ask what is the simplest model that captures some of the essential aspects of atmospheric convection. In this paper we look for such a minimal model and discuss a simple setting that describes the basic properties of atmospheric convection. The description is based on a classic model introduced by Prandtl [24], which represents a layer of dry air kept in statistically stationary radiative–convective equilibrium. Surprisingly, this model has been very little studied in atmospheric dynamics since then, and, to our knowledge, the full reference list is composed of the works of Deardorff and Islam *et al* [11, 19] and Robe and Emanuel [27]. Interestingly, this model is mathematically equivalent to the problem of a fluid layer that is cooled from above and is internally heated, as is thought to be the case for the Earth's mantle [7, 10, 26, 28, 29, 33, 34]. On the other hand, the value of the Reynolds number considered in mantle convection studies is usually much smaller than that for the atmosphere, and the value of the Prandtl number for mantle convection is definitely larger than that for air ($Pr = 0.7$ for atmospheric convection while $Pr \to \infty$ for mantle convection).

Before delving into the Prandtl convection problem, we mention a basic difference between pattern formation theory, as it is normally understood and to which this focus issue is devoted, and the study of strongly nonlinear structures such as those discussed in this paper. Traditionally, pattern formation refers to a regime that is little beyond the first linear instability of the system, and it can, in many circumstances, be described by a weakly nonlinear expansion of the full equations. Examples are abundant: in the realm of convection we cite the emergence of rolls in Rayleigh–Benard (RB) convection at values of the Rayleigh number just above critical [5, 21].

In contrast, coherent structures such as vortices and convective plumes (e.g., [4, 20, 22]) or spatio-temporal intermittency such as that of rainfall fields (e.g., [15] and references therein), emerge in the strongly nonlinear regime. As a consequence, their understanding does not generally follow from weakly nonlinear expansions of the equations of motion. The systematic description of these strongly nonlinear structures is far less advanced than pattern formation theory. Much of the work on strongly nonlinear coherent structures is experimental, observational and numerical, and we are still lacking a unified view of structure formation. Perhaps, also, there is not a unified view of strongly nonlinear structures, and each system has its own avenues and rules.

2. The Prandtl problem

We consider the setting introduced by Prandtl [24], which represents a layer of dry air that is radiatively cooled throughout its interior and is heated from below by a turbulent heat flux from a ground surface kept at constant temperature by solar radiation.

In equilibrium, the incoming solar radiation at the top of the atmospheric layer matches the total outgoing radiation. Transfer of heat from the ground to the overlying fluid destabilizes the latter, resulting in convection. The air is supposed to be transparent to the incoming short-wave solar radiation, while it absorbs and re-emits the long-wave radiation received from the ground.

The dynamics of this simplified system can be described by considering the details of the entropy balance [13, 14]. Starting from the first law of thermodynamics, one obtains

$$c_p \frac{\mathrm{d}\ln T}{\mathrm{d}t} - R_\mathrm{d} \frac{\mathrm{d}\ln p}{\mathrm{d}t} = \frac{Q_\mathrm{rad}}{T} + s_\mathrm{irr} \tag{1}$$

where c_p is the heat capacity at constant pressure, R_d is the gas constant for dry air, p is pressure, s_irr represents irreversible entropy sources and Q_rad is the radiative cooling rate. By averaging equation (1) over the entire domain and over a long enough time to average out statistical fluctuations, one obtains

$$\langle s_\mathrm{irr} \rangle = -\left\langle \frac{Q_\mathrm{rad}}{T} \right\rangle \tag{2}$$

where the symbol $\langle \cdot \rangle$ indicates an average over three-dimensional space and time. In statistical equilibrium, the heat flux entering from the bottom boundary is balanced by the radiative cooling in the bulk of the fluid. However, the heat input and output take place at two different temperatures, and this should be taken into account when evaluating the average of $\mathrm{d}Q_\mathrm{rad}/T$ in equation (2). This temperature difference leads to the expression

$$\langle s_\mathrm{irr} \rangle = \mathcal{F}_\mathrm{s} \left(\frac{1}{\langle T \rangle} - \frac{1}{T_\mathrm{s}} \right) \tag{3}$$

where $\mathcal{F}_\mathrm{s}$ is the net flux at the surface (and also the net radiative cooling in the fluid), T_s is the surface temperature (the temperature at which the heat enters the system) and $\langle T \rangle$ is the average temperature at which radiative cooling occurs[5].

Assuming for the moment that the dissipation of kinetic energy is the dominant irreversible entropy source, the left side of equation (3) is the average of the dissipative heating divided by temperature. In statistical equilibrium, dissipation of kinetic energy must be equal to the rate of conversion of potential to kinetic energy, $\langle wT' \rangle$, and thus we can write

$$\frac{1}{T_\mathrm{diss}} \langle wT' \rangle \propto F_\mathrm{s} \left(\frac{1}{\langle T \rangle} - \frac{1}{T_\mathrm{s}} \right) \tag{4}$$

where $\langle wT' \rangle$ is the average buoyancy flux and T_diss is the average temperature at which kinetic energy is dissipated (again we have confused the average of the inverse temperature with the inverse of the average temperature). This expression reveals that the average buoyancy flux is determined by the energy input into the system, and it can be interpreted as a thermodynamic efficiency. From the estimate of $\langle T \rangle$ for the atmosphere and assuming for simplicity that

[5] The correct average is $\langle 1/T \rangle$ instead of $1/\langle T \rangle$. However, at the level of this description the difference between these two quantities is small and we can use the simplest inverse of the average temperature instead of the average of $1/T$.

$T_{\rm diss} \approx \langle T \rangle$, one can estimate an appropriate scale for the buoyancy flux in the system. This scale is proportional to the radiation absorbed by the surface and to the difference between the surface temperature and a mean temperature of the free atmosphere. Convection thus works as a heat engine, that converts the heat absorbed at the surface into mechanical work of the fluid, with an efficiency determined by the difference between the input and output temperatures. No work is done on the environment, rather the mechanical energy is dissipated locally and is turned back into enthalpy.

3. The Prandtl problem for a layer of finite depth

The original formulation of the Prandtl problem refers to a domain that is infinitely extended in the horizontal plane (horizontal coordinates are herein denoted by x and y), and is semi-infinite along the vertical coordinate z: the domain is bounded from below by a rigid surface at $z = 0$ and it extends to $z \to \infty$. For the sake of simplicity, here we constrain the vertical extent of the system, and consider a fluid layer with depth $D = H + h$ confined between two horizontal plates. The domain is subdivided into two distinct sublayers: the first, with height H, represents the troposphere and it is uniformly cooled at a constant rate, Q_0. The second layer, with height h, represents the stratosphere and has no net radiative cooling (i.e. the upper layer is assumed to be either transparent to radiation or in a state of local radiative balance). The choice of a constant tropospheric cooling is consistent with measurements of atmospheric radiative fluxes, which provide approximately constant vertical profiles of radiative cooling rates in the troposphere [32].

The governing equations for this system are the momentum, energy and continuity equations which, for an incompressible fluid and in the Boussinesq approximation, are written as

$$\frac{\partial \boldsymbol{u}}{\partial t} + \boldsymbol{u} \cdot \nabla \boldsymbol{u} = -\frac{1}{\rho} \nabla p + \boldsymbol{g} \frac{\rho}{\rho_0} + \nu \nabla^2 \boldsymbol{u} \tag{5}$$

$$\frac{\partial T}{\partial t} + \boldsymbol{u} \cdot \nabla T = \kappa \nabla^2 T - \frac{Q_{\rm rad}}{c_p} \tag{6}$$

$$\nabla \cdot \boldsymbol{u} = 0 \tag{7}$$

where $\rho = \rho_0[1 - \alpha(T - T_0)]$ is the fluid density, T is temperature, $\boldsymbol{u} \equiv (u, v, w)$ is velocity and κ, ν and α are, respectively, the thermal diffusivity, kinematic viscosity and volumetric coefficient of thermal expansion of the fluid. The vertical velocity component is w and we have linearized the equation of state around the reference temperature T_* and the reference density $\rho_* \equiv \rho(T_*)$, consistent with the Boussinesq approximation[6].

The cooling term is defined as $-Q_{\rm rad}/c_p$ in the temperature equation, where $Q_{\rm rad} = Q_0$ for $0 \leq z \leq H$ and $Q_{\rm rad} = 0$ for $H \leq z \leq D$. For the velocity field, rigid (no slip) boundary conditions are used on both horizontal boundaries[7]. For the temperature field, flux boundary conditions are imposed:

[6] This is a significant simplification with respect to the properties of the real atmosphere. It would have been more realistic to retain the dependence of density on pressure, and use the so-called anelastic approximation instead of the Boussinesq approximation. On the other hand, for motions whose vertical extent does not exceed the scale height of the atmosphere, the error due to the use of the Boussinesq approximation is probably not worrisome, given the heuristic nature of the model adopted here.

$$F_{\text{bottom}} = -\kappa \frac{\partial T}{\partial z} = c(T_s - T|_{z=0}) \qquad \text{for } z = 0 \tag{8}$$

$$\frac{\partial T}{\partial z} = 0 \qquad \text{for } z = D \tag{9}$$

where T_s is a constant reference soil temperature (determined by the incoming solar radiation and by the soil albedo) and c is a turbulent velocity scale associated with the heat flux from the bottom boundary. The heat flux at the lower boundary of the fluid layer is proportional to the difference between the reference temperature of the soil, T_s, and the temperature of the lowermost layer of air, $T(z = 0)$. This condition at the lower boundary corresponds to assuming a rough lower plate. At the upper boundary, we impose insulating (zero flux) boundary conditions for the convective (turbulent) and conductive heat fluxes, while the radiation emitted by the lower layers is allowed to escape to outer space: we assume the system to be topped by an insulating but perfectly transparent plane. Periodic boundary conditions are used along the two horizontal directions. The ratio of the horizontal size of the periodic domain, L, to the vertical extent of the model troposphere, H, defines the aspect ratio of the system.

The above equations are made dimensionless by using the Prandtl scaling:

$$\tilde{x} = x/H$$
$$\tilde{t} = Ut/H$$
$$\tilde{u} = u/U$$
$$\tilde{p} = p/\rho_0 U^2$$
$$\tilde{T} = (T - T_s)/\Delta T$$

where

$$U = \left(\frac{g Q_0 H^2}{c_p T_s}\right)^{\frac{1}{3}} \tag{10}$$

$$\Delta T = \frac{U^2 T_s}{gH}. \tag{11}$$

Note, in particular, that the timescale used in the non-dimensional equations is the convective overturning scale, $\tau = H/U$, which defines the natural timescale for this problem. We have also assumed that $\alpha \approx 1/T \approx 1/T_s$.

In dimensionless variables, the equations of motion become

$$\frac{\partial \boldsymbol{u}}{\partial t} + \boldsymbol{u} \cdot \nabla \boldsymbol{u} = -\nabla p + T\hat{\boldsymbol{k}} + \frac{1}{Re}\nabla^2 \boldsymbol{u} \tag{12}$$

$$\frac{\partial T}{\partial t} + \boldsymbol{u} \cdot \nabla T = \frac{1}{RePr}\nabla^2 T - \theta(z_0 - z) \tag{13}$$

$$\nabla \cdot \boldsymbol{u} = 0 \tag{14}$$

[7] The no-slip boundary condition on the lower plate has a natural motivation as the lower boundary represents the ground. On the upper plate, the choice of the velocity boundary condition is more artificial, as there is no upper plate in the atmosphere. On the other hand, the dynamics in the upper layers of our model is much less intense than in the lower layers. For this reason, the upper boundary condition on velocity is less important. Here we have imposed a no-slip condition also on the upper plate. The use of a no-stress condition on the upper boundary does not significantly alter the results.

where $\theta(\zeta) = 1$ for $\zeta \geq 0$ and $\theta = 0$ otherwise, $z_0 = 1$ is the dimensionless height of the model tropopause and we have dropped the tilde decoration.

The boundary conditions for the velocity and temperature fields become

$$u = v = w = 0 \qquad \text{for } z = 0 \text{ and } z = 1 + \frac{h}{H}$$

$$\frac{\partial T}{\partial z} = \frac{c}{U} RePrT \qquad \text{for } z = 0$$

$$\frac{\partial T}{\partial z} = 0 \qquad \text{for } z = 1 + \frac{h}{H}$$

and the dynamics is governed by three non-dimensional parameters:

- the Reynolds number, $Re = UH/\nu$;
- the Prandtl number, $Pr = \nu/\kappa$;
- the ratio c/U between the velocity scale of the turbulent heat flux at the bottom boundary and the velocity scale of the convection.

The dimensionless equations are numerically integrated using a mixed spectral–finite-difference technique. In this approach, Fourier decomposition in both planar directions is associated with a finite difference scheme in the vertical direction. An explicit third-order Runge–Kutta integration scheme is used for time advancement.

Before closing this section, we note that the Prandtl convection setting discussed here is mathematically equivalent to the convection of a fluid layer that is heated internally and is cooled from above, provided we change the sign of the acceleration of gravity. The dynamics of an internally heated layer is of relevant interest for the study of mantle convection, and several results are available on this system (e.g., [7, 10, 26, 28, 29, 33, 34]). In the case of mantle convection, however, one is usually faced with relatively low values of the Reynolds number and (infinitely) large values of the Prandtl number, while for atmospheric convection one has $Pr = 0.7$ and $Re \to \infty$. In addition, for atmospheric convection the correct bottom boundary condition is on the flux, while most studies of mantle convection cope with a fixed temperature on the upper plate. Finally, in atmospheric convection one has to cope with the difference between the troposphere and the stratosphere, and the problem becomes one of penetrative convection.

4. Plumes in Prandtl convection

We consider one specific example of statistical radiative–convective equilibrium, for $Re = 100$, $Pr = 0.71$ and $c/U = 1.5 \times 10^{-3}$. The integration domain has size $10 \times 10 \times 1.5$ and a grid with $128 \times 128 \times 145$ mesh points. Note that the above value of Re should be interpreted as an 'eddy' value: the dissipation and the thermal conductivity represent turbulent eddy quantities rather than molecular values. The simulation discussed here could thus be interpreted as a LES (large eddy simulation) with the simplest possible closure scheme (i.e. eddy viscosity) rather than a DNS (direct numerical simulation).

To provide physical scales for this problem (see figure 1), we fix the dimensional height of the troposphere as $H = 10$ km and the turbulent velocity scale at the bottom as $c = 10^{-2}$ m s^{-1}. Thus, the mid tropospheric level in the model, $z = 0.5$, corresponds to an altitude of about 5000 m above the ground. Since the aspect ratio of this simulation is 10, the value of H implies that

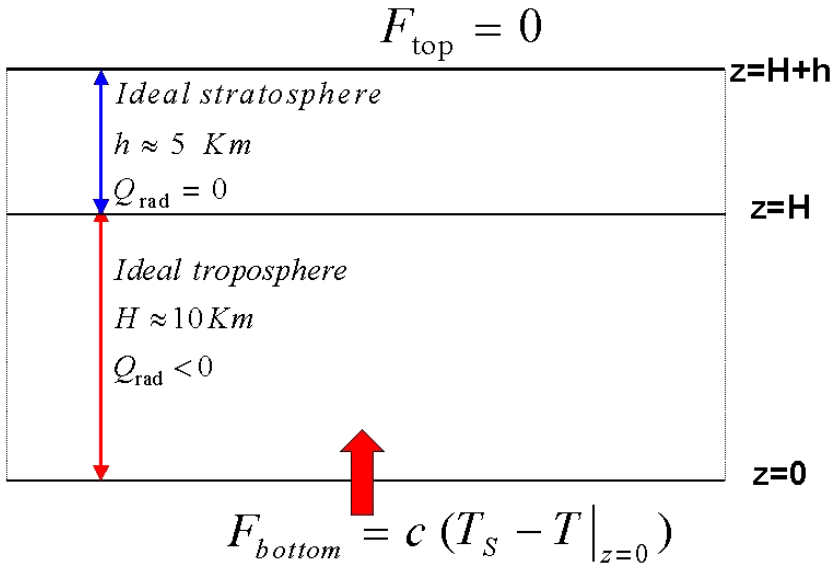

Figure 1. The setting of the (modified) Prandtl problem, as implemented in this work.

the horizontal size of the simulation domain is $L = 100$ km. With these choices, the convective velocity timescale is $U \approx 6.7$ m s^{-1} and the convective timescale is $\tau = H/U = 1500$ s.

The total average heat flux in the system, $\bar{\mathcal{H}}$, is defined as the sum of the average convective, conductive and radiative heat fluxes, i.e.

$$\bar{\mathcal{H}} = \bar{\mathcal{H}}_t + \bar{\mathcal{H}}_{\text{cond}} + \bar{\mathcal{H}}_{\text{rad}} \tag{15}$$

where the average convective (turbulent) heat flux is

$$\bar{\mathcal{H}}_t = \overline{wT'} \tag{16}$$

and the average conductive heat flux is

$$\bar{\mathcal{H}}_{\text{cond}} = -\frac{1}{RePr}\frac{\partial \bar{T}}{\partial z}. \tag{17}$$

Here $T' = T - \overline{T(z)}$ is the temperature perturbation and $\overline{T(z)}$ is the average temperature at height z. The overbar indicates average over horizontal directions and over time. In dimensionless variables, the average radiative heat flux is

$$\bar{\mathcal{H}}_{\text{rad}} = \int_0^z \theta(1 - z')\,\mathrm{d}z'. \tag{18}$$

This gives $\bar{\mathcal{H}}_{\text{rad}} = z$ for $0 \le z \le 1$ and $\bar{\mathcal{H}}_{\text{rad}} = 1$ for $1 < z \le 1 + h/H$. Since the total average heat flux in the system is constant along the vertical, the 'kinetic' portion of the average heat flux, $\bar{\mathcal{H}}_t + \bar{\mathcal{H}}_{\text{cond}}$, displays a linear decrease with height in the model troposphere and it becomes zero close to the model tropopause. Outside the bottom boundary layer, the contribution from the convective heat flux dominates over heat conduction.

When statistical radiative–convective equilibrium is achieved, the convecting fluid is separated into two different regions: a thermal boundary-layer close to the surface, where the

average temperature decreases rapidly with height, and the well-mixed fluid in the bulk of the model troposphere, where the average temperature becomes independent of height.

Physically, the heat flux from the bottom tends to increase the temperature of the troposphere, and radiative cooling removes the heat coming from the lower layers. In the absence of convective mixing, one would obtain a stationary solution with the average temperature decreasing quadratically with height. The presence of convection mixes the fluid and makes the average temperature homogeneous, similarly to what happens in RB convection at large enough Rayleigh number. Interestingly, approximately isothermal conditions persist in most of the model stratosphere. The isothermal profile is indeed a solution of the stationary problem for a transparent fluid layer with fixed bottom temperature and insulating upper boundary. Thus, the temperature of the model stratosphere adjusts itself to the temperature of the uppermost layer of the model troposphere, and an approximately constant average temperature is observed throughout the fluid above the bottom boundary layer. A weaker boundary layer is present close to the upper plate.

Figure 2 shows the average vertical temperature profile and the vertical profile of the kinetic part of the total heat flux. Both profiles are obtained by averaging over the horizontal and over a number of time steps corresponding approximately to 30 convective times, τ.

To illustrate the structure of the convective overturning, in figures 3–5 we show horizontal cross sections of the vertical velocity, w, of the temperature perturbation, T', and of the convective heat flux, $\mathcal{H}_t = wT'$, at three reference heights. The horizontal cross sections are taken at $z = 0.08$, in the bottom boundary layer, at $z = 0.5$, in the middle of the model troposphere, and at $z = 1.25$, above the model tropopause.

In the bottom boundary layer, the convection is organized in lines that are approximately straight and form polygonals. In the core of the model troposphere, a characteristic spoke pattern of rising motions is present. The hubs of the spoke pattern are the centres of most energetic ascents. Although some elongated features are still present at $z = 0.5$, there is a predominance of isolated plumes that springs from the hubs of the spoke pattern. The remaining part of the domain is characterized by cold air that is slowly subsiding. The plumes that survive the journey to the top of the model troposphere penetrate into the stratosphere, causing entrainment. This penetration is quite weak, explaining the characteristic total heat flux profile shown before. A vertical cross section (figure 6) confirms that the convective heat flux is dominated by a few ascending structures surrounded by slowly subsiding air, and that only the more intense plumes penetrate into the model stratosphere. Note, also, that the more intense structures identified in the heat flux field are associated with the largest values of the vertical velocity field. Interestingly, a similar organization of large-scale convective elements over the intersection of surface convergence features has been detected in studies of mesoscale storm organization [9].

The spatial organization observed in the Prandtl model is quite different from the typical behaviour of RB convection. In the latter, the intrinsic up–down symmetry of the system produces both hot updrafts and cold downdrafts, which on average occupy the same portion of space. The collision of cold downdrafts with the hot bottom boundary layer (and, vice versa, the collision of hot updrafts with the cold top boundary layer) is a crucial aspect of plume dynamics in RB convection (see, e.g., [8, 30, 31]). In the Prandtl setting, the presence of radiative cooling and the difference in the upper and lower boundary conditions break the up–down symmetry. There are no cold downdrafts impinging on the bottom boundary layer, and the hot updrafts lose most of their strength before reaching the top boundary. As a result, the overall field is dominated by a few intense updrafts of warm air that hardly penetrate the model stratosphere, and by a

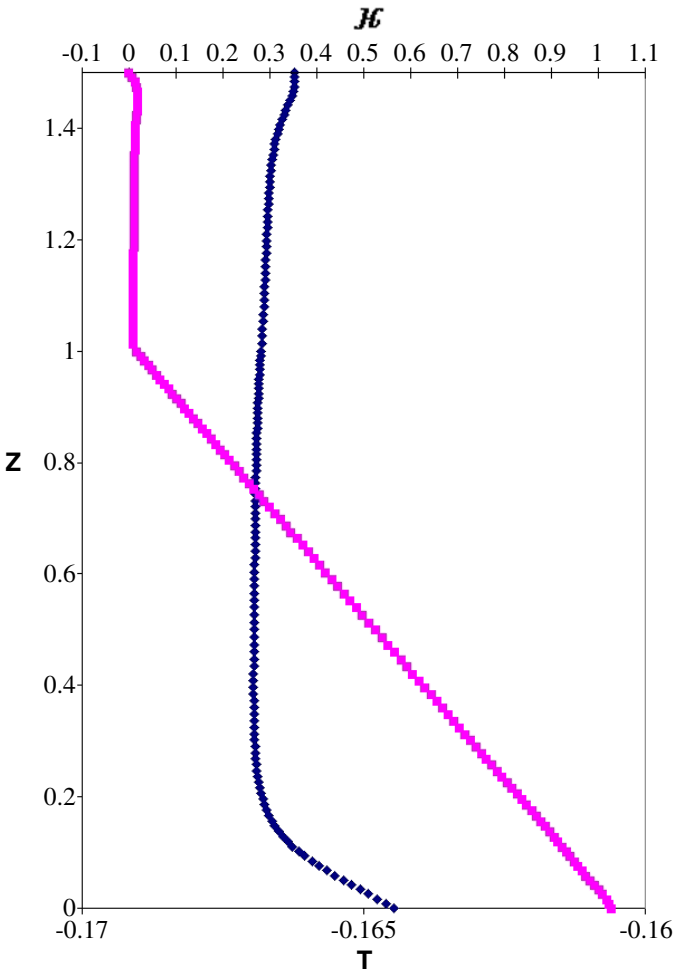

Figure 2. Time-averaged temperature profile (blue curve) and time-averaged profile of the sum of the convective and conductive heat fluxes (purple curve). The (non-dimensional) temperature profile has been divided by the (non-dimensional) soil temperature $T_s/\Delta T$.

general slow subsidence of cool air, similar to what is observed in atmospheric convection. For this reason, we believe that the Prandtl model is one of the simplest settings that includes the essential elements of atmospheric convection.

5. Intermittency of the heat flux field

In the following we explore some of the elementary statistical properties of the heat flux field, and, in particular, its intermittency properties. Figure 7 shows the horizontal power spectrum, $P(k)$, of the heat flux field at $z = 0.5$, obtained as an average over 30 convective timescales. Here we show the spectrum along the x direction; owing to isotropy the spectrum along y is approximately the same. The spectrum displays a steep decrease at small wavelength (the straight line in the figure shows a power-law decrease $P(k) \propto k^{-5}$ for comparison), and a flat plateau at larger scales. The transition happens at a scale of about $0.1L$, corresponding to about 10 km. This value marks

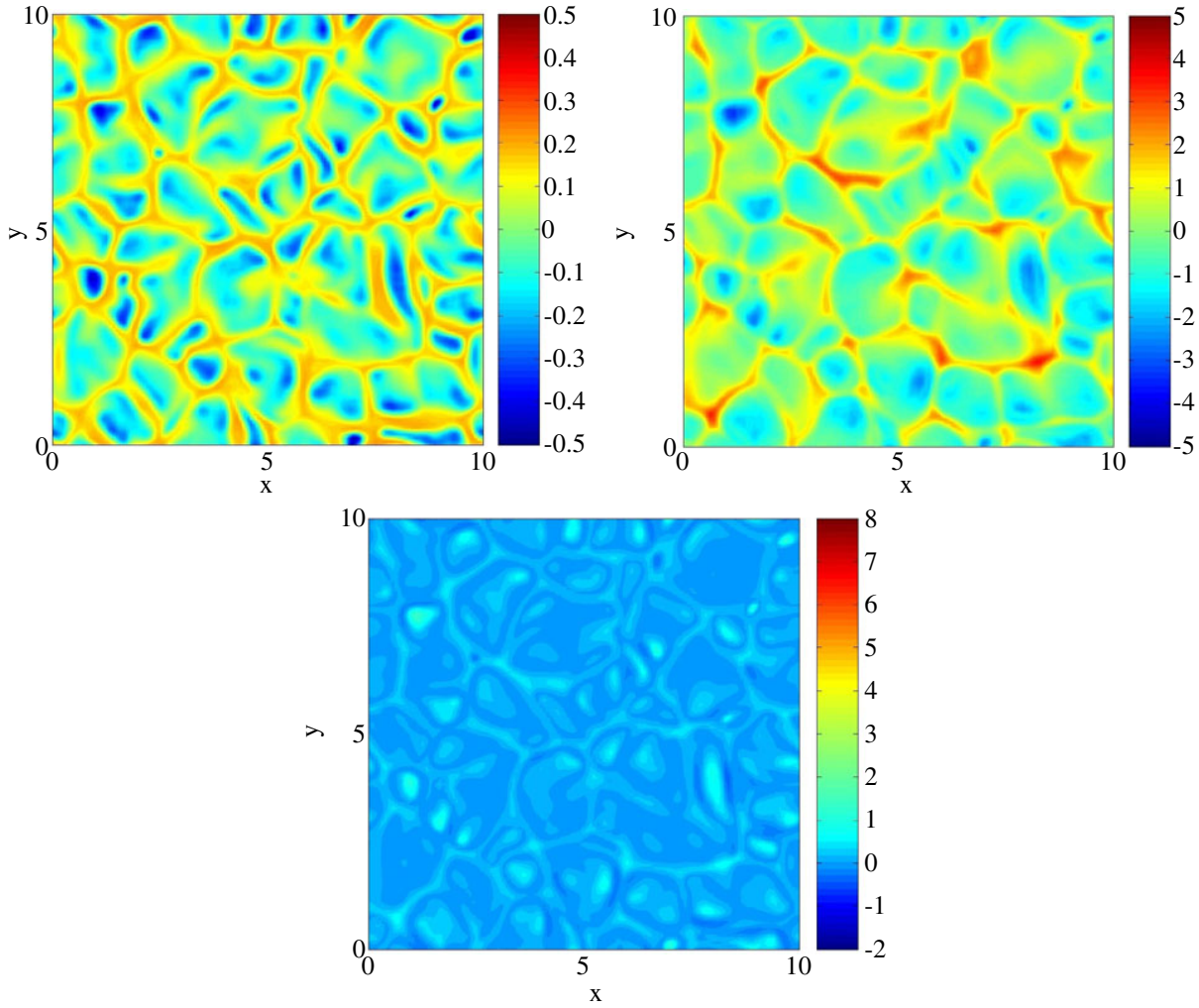

Figure 3. Horizontal cross sections of the vertical velocity (top left panel), of the temperature perturbation (top right panel), and of the convective heat flux (bottom panel) at $z = 0.08$, in the bottom boundary layer.

the transition from the scale of the individual plumes, whose lateral size does not exceed the height of the troposphere, and the dynamics at larger scales, dominated by an approximately homogeneous distribution of individual plumes. Compared with the atmosphere, this version of the Prandtl model lacks large-scale organization (such as that generated by mesoscale complexes, squall lines, or cyclonic circulations) as well as the clustering of the individual plumes into plume complexes (e.g., the small mesoscale areas observed in convective precipitation, see [1]).

Figure 8 shows the probability density function (PDF) of the convective heat flux intensity at level $z = 0.5$, obtained from an average over 30 convective timescales. The PDF of $\mathcal{H}_t$ confirms the strongly skewed nature of the heat flux field, with an elongated tail for large positive values of $\mathcal{H}_t$. This is to be contrasted with the case of RB convection, where the heat flux has a symmetric distribution. The long positive tail of the PDF of $\mathcal{H}_t$ is due to the intermittent nature of the heat flux field, and it is associated with the predominance of the strong convective updrafts that carry most of the heat flux from the lower levels to the top of the model troposphere.

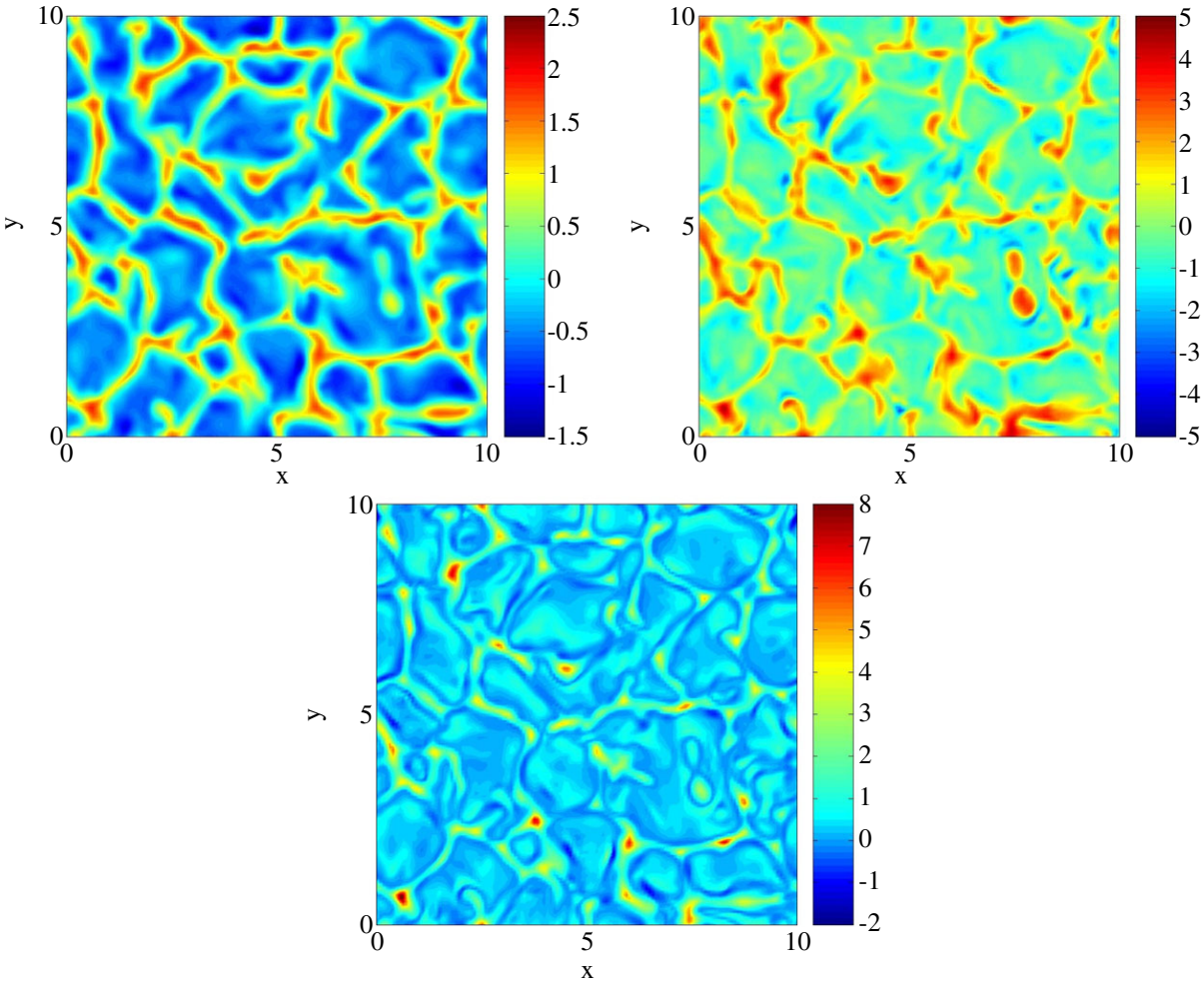

Figure 4. Horizontal cross sections of the vertical velocity (top left panel), of the temperature perturbation (top right panel), and of the convective heat flux (bottom panel) at $z = 0.5$, in the core of the model troposphere.

The spectrum of generalized fractal dimensions provides further information on the intermittency of the heat flux field. Consider a two-dimensional field, $\Psi(x, y)$, discretized on a regular grid. First, we need to define a measure, $\varepsilon(x, y)$, on this field (in the case of a positive-definite field, the measure can be the field itself, i.e. $\varepsilon = \Psi$). We define the integral of the measure, $\mu_j(\lambda)$, as the integral of ε on an area with linear size λ, centred on the point (x_j, y_j). We define the partition functions, $Z(\lambda, q)$, as

$$Z(\lambda, q) = \sum_j \mu_j(\lambda)^q, \tag{19}$$

where $q \geq 0$. For random fields with scaling properties, in the limit for $\lambda \to 0$ one has

$$Z(\lambda, q) \sim \lambda^{\tau(q)}. \tag{20}$$

For 'physical' fractals, the power-law behaviour extends only on a finite range of values of λ, and the exponent $\tau(q)$ is usually obtained by a least-squares-fit of $\log Z$ versus $\log \lambda$ in the scaling range. The generalized fractal dimensions, $D(q)$, are obtained from $\tau(q)$ as [17]

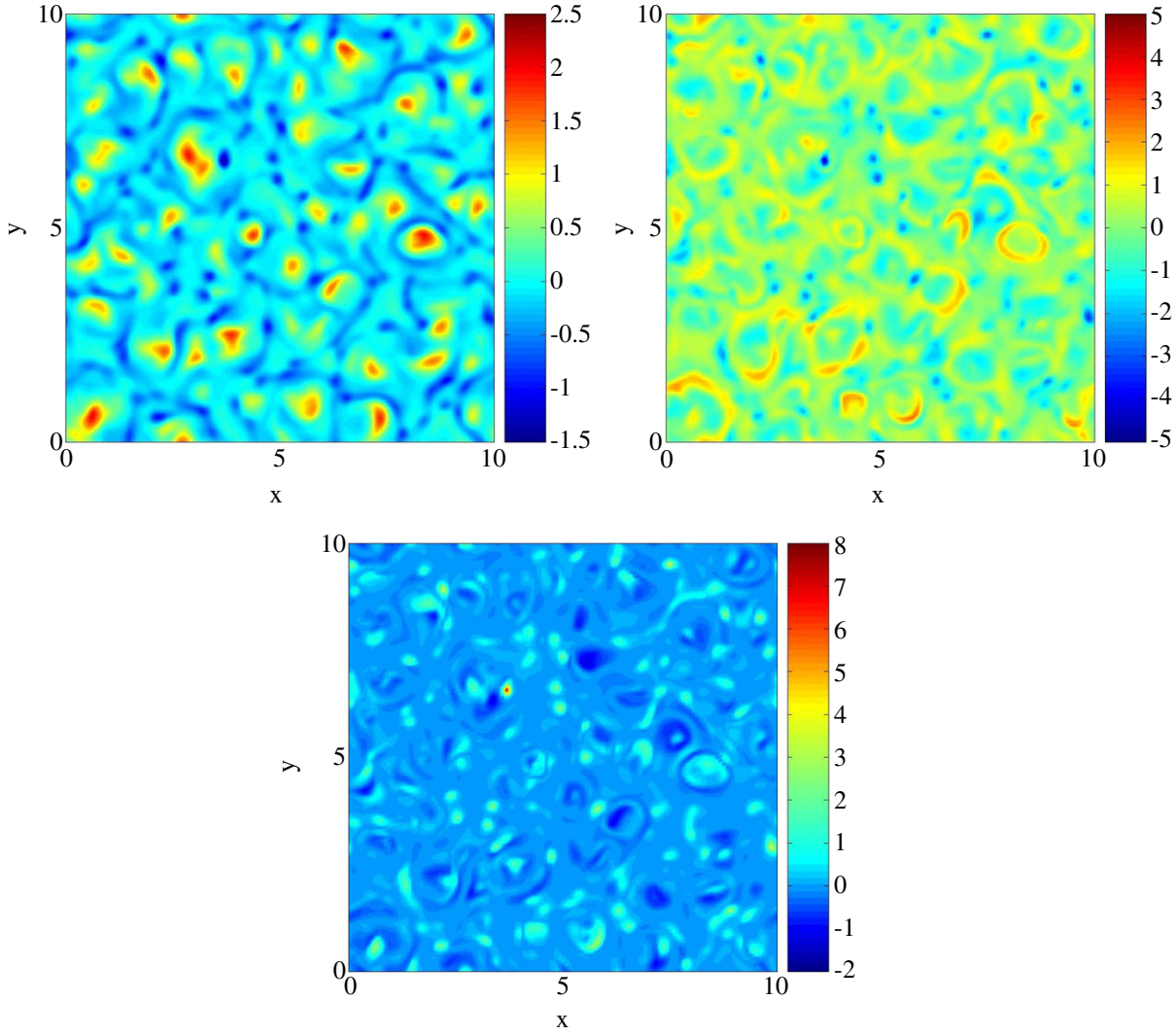

Figure 5. Horizontal cross sections of the vertical velocity (top left panel), of the temperature perturbation (top right panel), and of the convective heat flux (bottom panel) at $z = 1.25$, in the lower model stratosphere.

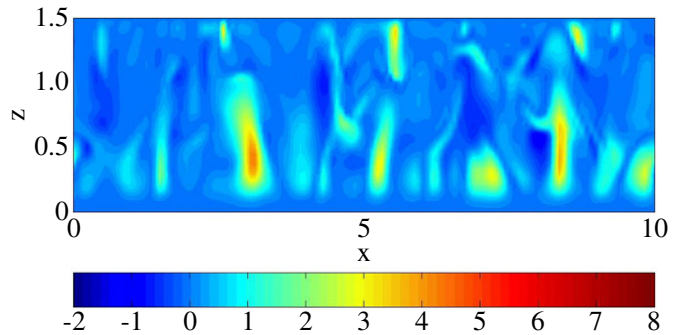

Figure 6. Vertical cross section of the convective heat flux field at $y = 0$.

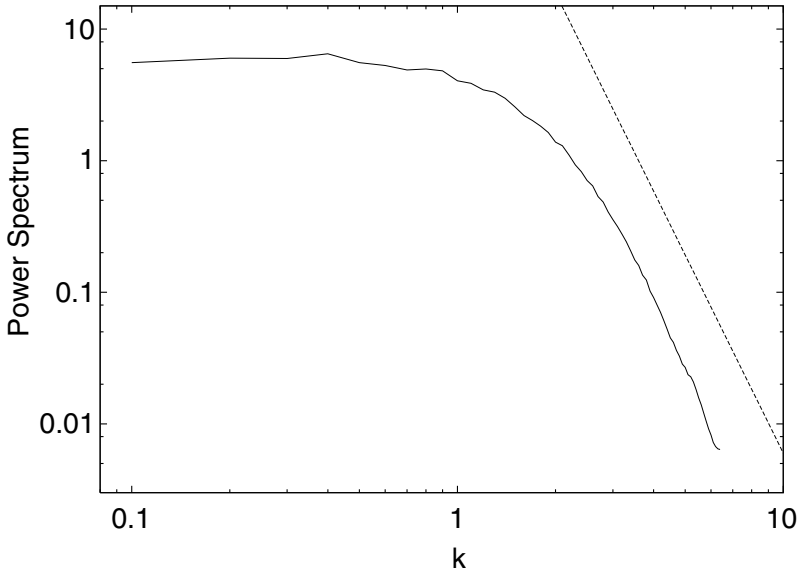

Figure 7. Horizontal power spectrum, $P(k)$, of the heat flux field at $z = 0.5$. The line indicates a power law k^{-5} for comparison.

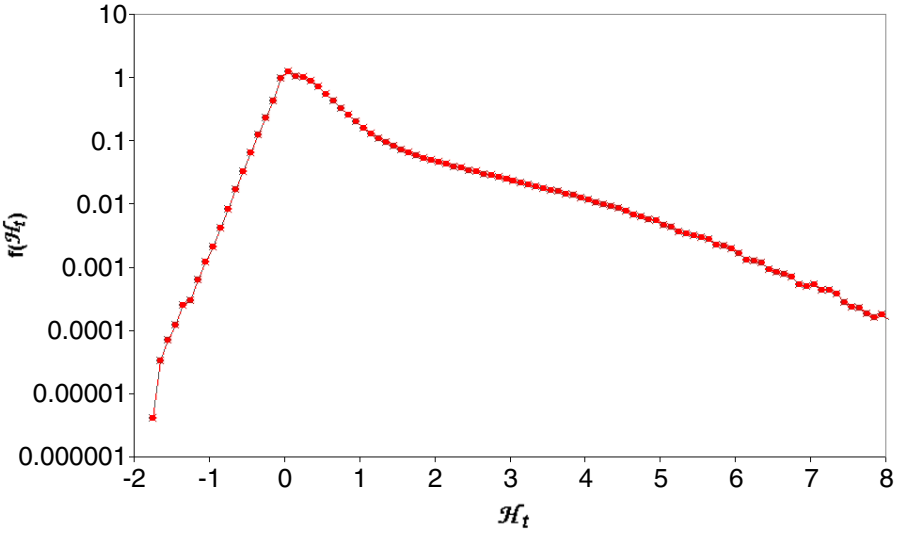

Figure 8. PDF of the convective heat flux at $z = 0.5$.

$$D(q) = \frac{\tau(q)}{q-1}. \tag{21}$$

For $q = 0$, one finds the box-counting dimension, $D(0)$. This represents the fractal dimension of the support where the field is different from zero. For $q = 2$, one finds the correlation dimension, $D(2)$. Fields characterized by $D(q) = D(0)$ for any q are said to possess simple scaling or to be 'monofractal', while scaling fields characterized by $D(q) < D(q')$ for $q > q'$ are said to possess anomalous scaling, or to be 'multifractal'. Multifractality is a sign of intermittency, i.e. of the fact that higher-order moments are more rare and more intense than for a Gaussian field.

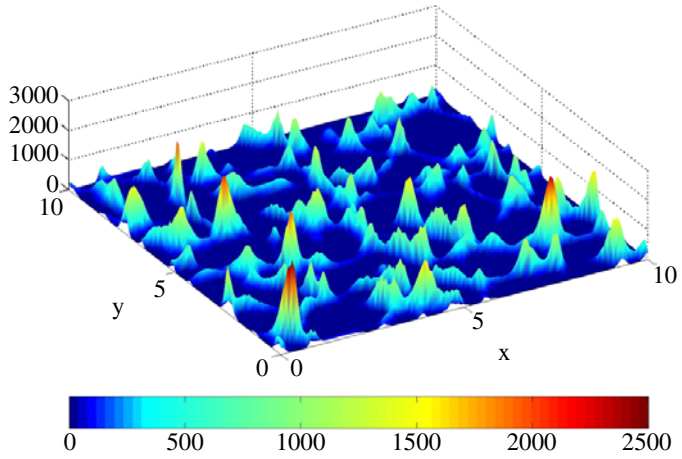

Figure 9. Vertically- and time-integrated warm updraft field obtained from the Prandtl model.

To apply the box-counting method to the heat flux we need first to define a positive measure on the field. In the following, we focus on the properties of the upward flux of warm air, a measure that is dominated by the behaviour of the intense convective plumes that spring from the lower boundary layer and reach the tropopause. In the Prandtl setting, this flux represents the main component of the turbulent heat transport from the warmed ground toward the cooler upper atmospheric layers.

Since the plumes display remarkable coherence along the vertical direction, and a very limited tilt of their axis (owing to the lack of vertical shear in this model), we consider the time- and vertically-integrated upward flux of warm air, ϵ, as

$$\epsilon(x, y, t) = \int_{t-\Delta t}^{t} \mathrm{d}t \int_{z_\mathrm{B}}^{z_\mathrm{TP}} \mathcal{H}_\mathrm{t}^{+} \, \mathrm{d}z \tag{22}$$

where Δt is the cumulation time, z_B is the height of the bottom boundary layer, and z_TP is the height of the model tropopause. The upward flux of warm air, $\mathcal{H}_\mathrm{t}^{+}$, is defined as that portion of the convective heat flux, $\mathcal{H}_\mathrm{t} = wT'$, which is characterized by $w > 0$ and $T' > 0$.

Figure 9 shows one snapshot of $\epsilon(x, y, t)$ obtained from the Prandtl model, using—in dimensional variables—$\Delta t = 15$ min, $z_\mathrm{B} = 2$ km, and $z_\mathrm{TP} = 10$ km. (Choosing other cumulation times between about 2 and 30 min provides analogous results.) The field of updrafts is characterized by localized, intense peaks separated by large areas of low or zero activity and connected to each other by lines of lower flux intensity. Although the present version of the Prandtl model does not contain any moisture, it is tempting to interpret these intense plumes as a dry analogue of the convective updrafts that are at the origin of strong rainfall cells.

Figure 10 shows the set of generalized fractal dimensions for the measure $\epsilon(x, y)$; the results are obtained by averaging the generalized dimensions of the individual fields over 30 convective times. The positive heat flux field in this radiative–convective system displays anomalous scaling and intermittency, as indicated by the fact that the generalized dimensions $D(q)$ decrease for increasing moment order q. We recall that fields of intense convective precipitation also display anomalous scaling (e.g., [15]). The results reported here suggest that the origin of rainfall intermittency may reside in the dynamical properties of the field of convective updrafts. Further analyses of simplified moist convective systems will hopefully elucidate this issue.

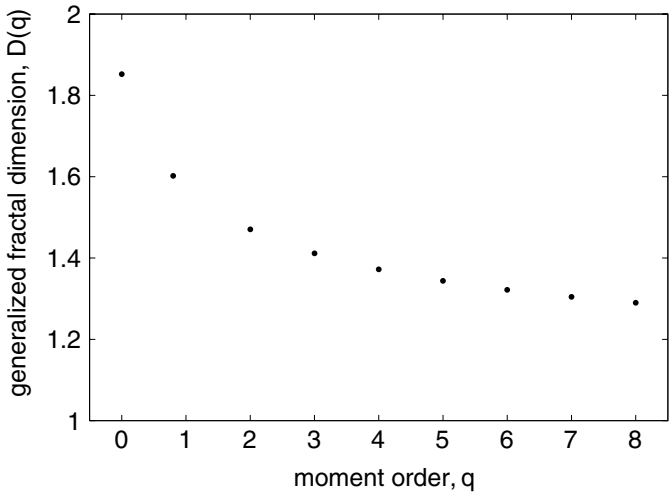

Figure 10. Generalized fractal dimensions for the (vertically- and time-integrated) warm updraft field obtained from the Prandtl model.

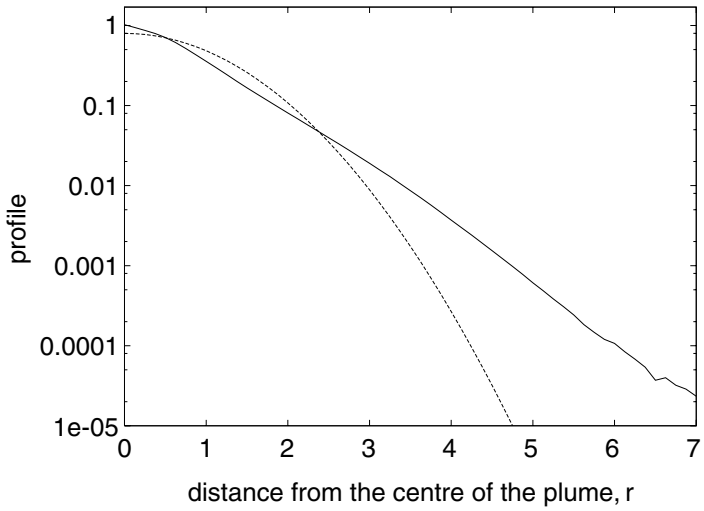

Figure 11. Average radial profile of the warm convective updrafts produced by the Prandtl model. The dashed curve shows a Gaussian profile for comparison.

A final point concerns the profile of the individual convective updrafts in the Prandtl problem. In figure 11 we show the average radial dependence of ϵ in convective plumes. For each of the intense updrafts present at a given time, we computed the shape of the field $\epsilon(x, y)$ around the local maximum (that defines the centre of the plume). The different updrafts were normalized to having the same integral and the same radius, and then averaged. A further azimuthal average around the centre of the updraft provides the mean profile. The average profile is closer to an exponential than to a Gaussian, again in agreement with what has been found for the shape of convective precipitation cells [16].

6. Summary and discussion

Convection plays a central role in pattern formation theories. The concept of pattern immediately brings to one's mind the picture of hexagonal convection rolls, and the experiments of Benard [2] are taken as paradigms of pattern formation studies. Similarly, the theoretical investigation of Rayleigh [25] paved the way to linear stability studies and to the mathematical understanding of the instabilities that generate patterns.

Since then, the convective motion of an incompressible fluid layer bounded by two solid horizontal surfaces kept at constant temperature—now called 'RB convection'—has become an evergreen of pattern formation. One of the reasons for which the RB setting has received so much attention is that its linear stability structure is quite simple, and so are the subsequent weakly nonlinear expansions. For this system, the entire sequence of transitions from linear instability, to weakly nonlinear roll structures, to pattern dynamics, spatio-temporal chaos, routes to turbulence, and finally fully developed turbulence has been thoroughly investigated: see e.g. [6, 31] and [3] for recent (and almost recent) reviews of RB convection.

As a model of atmospheric convection, however, the standard RB setting is not especially appropriate. One reason is that this configuration is up–down symmetric, a fact that is rarely observed in the oceans and the atmosphere where the upper and lower boundary conditions are usually different. Another important point is that most implementations of RB convection deal with fixed-temperature boundary conditions, while in most atmospheric situations one has to cope with boundary conditions on the heat flux rather than on temperature. Other effects can play an important role, such as rotation, the presence of dissolved salt in sea water, and the presence of moisture in the atmosphere. Additionally, air is not incompressible. Perhaps more importantly, the atmosphere is capable of absorbing and emitting electromagnetic radiation, and radiative heat transfer cannot be neglected.

For these reasons, we think it can be of some interest to move beyond the RB setting, and consider other forms of convective motion that are closer to the behaviour of the atmosphere. In this work we have discussed a simple model of radiative–convective dynamics, introduced by Prandtl in 1925, which we believe can improve our understanding of intense atmospheric convection. The model is highly idealized, and it should be taken just as a small step from the basic RB setting towards a closer description of atmospheric phenomena. In this paper, we have introduced the model and discussed some of the properties of the field of convective plumes that characterize the dynamics of this system. Future work will have to consider the role of wind shear, as well as the introduction of an active moisture field.

Acknowledgments

We benefited from many interesting discussions with Sandro Calmanti, Jost von Hardenberg, Claudia Pasquero, Giuseppe Passoni, Franco Siccardi and Edward A Spiegel, whom we gratefully acknowledge. We are grateful to an anonymous referee who pointed us to the analogy with mantle convection. Part of this work was conducted during our stay at the WHOI Summer Program on Geophysical Fluid Dynamics in summer 2001, and during the stay of A Parodi at EAPS-MIT. During these periods, A Parodi was supported by a CNR fellowship. This work is partially supported by GNDCI-CNR grants on rainfall downscaling and on applied research in meteohydrology.

References

[1] Austin P M and Houze R A 1972 *J. Appl. Meteorol.* **11** 926
[2] Benard H 1900 *Rev. Gen. Sci. Pures Appl.* **11** 1261
Benard H 1900 *Rev. Gen. Sci. Pures Appl.* **11** 1309
[3] Bodenschatz E, Pesch W and Ahlers G 2000 *Ann. Rev. Fluid Mech.* **32** 709
[4] Bracco A, McWilliams J C, Murante G, Provenzale A and Weiss J B 2000 *Phys. Fluids* **12** 2931
[5] Busse F 1967 *J. Fluid Mech.* **28** 223
[6] Busse F 1989 *Mantle Convection: Plate Tectonics and Global Dynamics* ed W R Peltier (New York: Gordon and Breach)
[7] Busse F and Riahi N 1982 *J. Fluid Mech.* **123** 283
[8] Castaing B, Gunaratne G, Heslot G, Kadanoff F, Libchaber A, Thomae S, Wu X-Z, Zaleski S and Zanetti G 1989 *J. Fluid Mech.* **204** 1
[9] Clark T L 1979 *J. Atmos. Sci.* **36** 2191
[10] Clever R M 1977 *J. Appl. Math. Phys. (ZAMP)* **28** 585
[11] Deardorff J W 1972 *J. Atmos. Sci.* **29** 91
[12] Emanuel K A 1994 *Atmospheric Convection* (New York: Oxford University Press)
[13] Emanuel K A 2000 *General Circulation Model Development* (New York: Academic)
[14] Emanuel K A and Bister M 1996 *J. Atmos. Sci.* **53** 3276
[15] Ferraris L, Gabellani G, Parodi U, Rebora N, von Hardenberg J and Provenzale A 2003 *J. Hydrometeorol.* **4** 544
[16] von Hardenberg J, Ferraris L and Provenzale A 2003 *Geophysical Research Abstracts* vol 5 EGS-AGU-EUG Joint Assembly
[17] Hentschel H G E and Procaccia I 1983 *Physica* D **8** 435
[18] Houze R A Jr 1993 *Cloud Dynamics* (San Diego, CA: Academic)
[19] Islam S, Bras R L and Emanuel K A 1993 *J. Appl. Meteorol.* **32** 297–310
[20] Julien K, Legg S, McWilliams J C and Werne J 1996 *J. Fluid Mech.* **322** 243
[21] Malkus W V R and Veronis G 1958 *J. Fluid Mech.* **4** 225
[22] McWilliams J C 1984 *J. Fluid Mech.* **146** 21
[23] Provenzale A 1999 *Annu. Rev. Fluid Mech.* **31** 55
[24] Prandtl L 1925 *Z. Angew. Math. Mech.* **5** 136
[25] Rayleigh L 1916 *Phil. Mag.* **32** 529
[26] Riahi N, Geiger G and Busse F 1982 *Geophys. Astrophys. Fluid Dyn.* **20** 307
[27] Robe F and Emanuel K A 1996 *J. Atmos. Sci.* **53** 3265
[28] Roberts P H 1967 *J. Fluid Mech.* **30** 33
[29] Schubert G, Glatzmaier G A and Travis B 1993 *Phys. Fluids* A **5** 1928
[30] Shraiman B and Siggia E D 1990 *Phys. Rev.* A **42** 3560
[31] Siggia E D 1994 *Annu. Rev. Fluid Mech.* **26** 137
[32] Smith W L, Shen W C and Howell H B 1977 *J. Appl. Meteorol.* **16** 384
[33] Tveitered M and Palm E 1976 *J. Fluid Mech.* **76** 481
[34] Tveitered M 1978 *Int. J. Heat Mass Transfer* **21** 335
[35] Zhang J, Childress S and Libchaber A 1997 *Phys. Fluids* **9** 1034